FP2.58 AN INVESTIGATION INTO GRADIENT BALANCE OF FLIGHT-LEVEL TROPICAL CYCLONE WINDFIELDS

Michael Gibbons*, Craig Miller
Boundary Layer Wind Tunnel Laboratory, University of Western Ontario, London, Canada

1. INTRODUCTION

Much debate has taken place surrounding gradient balance at the 700 and 850 hPa pressure levels in tropical cyclones. The work of Gray, Willoughby, Kepert and others have shown conflicting results regarding gradient balance. Willoughby's studies (1990, 1991) noted the presence of gradient balance for a selection of storms when the geopotential field is averaged in the azimuthal direction. Gray (1991) countered this claim by showing that, when plotted against the ratio of radio to radius to maximum wind (RMW), his selected storms were not in gradient balance. More recently, Kepert (2006a, 2006b) has studied two tropical cyclones in-depth: Hurricanes Georges 1998 and Mitch 1998. Kepert found that Hurricane Georges was in gradient balance whereas Hurricane Mitch was not.

Gradient balance is when three quantities are balanced within a rotating system: velocity, Coriolis acceleration, and pressure gradient. Gradient balance is an idealized process that offers a solution to the Navier-Stokes equations and is given as:

$$\frac{v^2}{r} + fv = \frac{1}{\rho}\frac{\partial p}{\partial r}, \qquad (1)$$

where tangential velocity is denoted by v, radius from the centre of rotation is denoted by r, the Coriolis parameter is denoted by f, and pressure is denoted by p.

This study builds upon the work of Willoughby, Grey and Kepert to further investigate gradient balance within the upper level of tropical cyclones. The presence of gradient balance will be classified by storm parameters in order to better understand when and where gradient balance occurs. The current study looks at 13 named storms between 2002 and 2008, with the intent of expanding this to 30 in the future. The 700 hPa pressure level has been investigated exclusively.

Using reconnaissance flight data it is possible to determine the centres of tropical cyclones and create complete two dimensional fields for quantities such as velocity and geopotential. Gradient balance can be assessed within a tropical cyclone using the geopotential and velocity fields. In this case, because the reconnaissance flights are flown at a constant pressure, the geopotential gradient replaces the pressure gradient in the gradient balance equation given by:

$$\frac{1}{\rho}\frac{\partial p}{\partial r} = \frac{\partial \Phi}{\partial r} \qquad (2)$$

where the geopotential height is given by Φ.

The analysis procedure is as follows. Using the reconnaissance flight data, high precision tropical cyclone centre fixes were created, and from these fixes continuous tracks were created. These tracks allowed the reconnaissance fight data to be converted from an earth relative to a storm centre relative coordinate system. The storm centre relative data was then objectively analyzed to create a continuous surface for geopotential height and velocity. The gradient balance equation is then used to calculate velocity based upon the geopotential gradient. These gradient balance velocities are then compared to the reconnaissance flight velocities so that gradient balance can be assessed. The presence of gradient balance will be categorized according to the following storm parameters: quadrant, central pressure and the change in the strength of the storm. Classifications were also made with respect to the radius and to the radius to maximum wind (RMW).

2. STORM TRACKS

There are a variety of methods that can be used to find centres of tropical cyclones. This study compared two methods that use reconnaissance flight data to determine the storm centres.

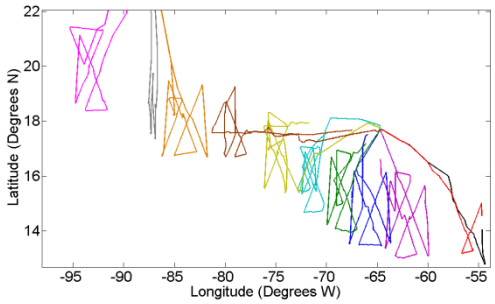

FIG. **1: Reconnaissance flights for Hurricane Dean (2007). These flights are used to determine tropical cyclone centres, which are then used to create a continuous track so that the centre of the storm can be determined at anytime.**

The first method was devised by Willoughby and Chen (1982, henceforth WC) and relies on a linear least squares minimization of velocity data to find the centre. The WC algorithm uses the wind direction to determine the centre of the storm. The algorithm first determines which data point is closest to the centre of the storm by defining a closeness parameter, *H*. As the radial distance from the centre of the storm is decreased, the geopotential height deficit value, *D*, and velocity decrease until they reach a minimum at the centre. *H* is given by:

$$H = gD + v^2 \qquad (3)$$

Corresponding Author Address: Mr. Michael Gibbons, Boundary Layer Wind Tunnel Laboratory, University of Western Ontario, London, Ontario, N6A 5B9. Email: mgibbo@uwo.ca

Lines tangent to the wind direction are defined as lines of position and these lines intersect with each other in the general location of the centre of the storm. The line of position corresponding to the minimized value of H is intersected with the lines of position within 5 km of this point, which creates a point cloud in the general location of the centre of the storm. A linear least squares analysis can then be carried out to determine an estimate of the centre of the storm.

The WC algorithm uses the aircraft coordinates and wind direction to calculate the distance between the intersected point and the unknown centre of the storm. This can be found, according to:

$$s_n = (X_n - X_C)\sin\theta_n + (Y_n - Y_C)\cos\theta_n \quad (4)$$

where s_n is the distance from the intersected point to the centre of the storm for data point n, (X_n, Y_n) is the aircraft coordinates for data point *'n'*, θ_n is the wind direction for data point n and (X_C, Y_C) is the location of the centre of the storm. The weighted root mean square value for s_n can be calculated and minimized, which determines the centre of the storm.

$$S_L^2 = (\sum W_n)^{-1} \sum W_n s_n^2 \quad (5)$$

$$\frac{\partial S_L^2}{\partial X_C} = 0 \quad (6)$$

$$\frac{\partial S_L^2}{\partial Y_C} = 0 \quad (7)$$

In the above equations, S_L^2 is the weighted RMS value of s_n and W_n is a weighting factor, which was determined by WC by trial and error. W_n is 10 when s_n is calculated at the minimized value of H and 1 otherwise.

If (2) is substituted into (3), and (4) and (5) are applied to (3), the location where the weighted RMS error for the centre of the storm is minimized can be determined. The equations that result from (4) and (5) are given below.

$$Y_C = \frac{1}{n}(\sum W_n)^{-1} \sum (W_n \sec(\theta_n)\ ((X_n - X_C)\sin(\theta_n) + Y_n \cos(\theta_n)) \quad (8)$$

$$X_C = \frac{1}{n}(\sum W_n)^{-1} \sum (W_n \csc(\theta_n)\ ((Y_n - Y_C)\cos(\theta_n) + X_n \sin(\theta_n)) \quad (9)$$

X_C and Y_C can be solved for directly so numerical methods are not required to solve (8) and (9). The advantages of this method are that they provide an explicit solution for the storm centres as the minimization yields a unique solution.

The second method is described by Kepert (2005) and implements a non-linear least squares minimization of pressure data to determine the centre of the tropical cyclone. Kepert referred to it as the Translating Pressure Fit (TPF) method and this nomenclature will be used here as well. The advantage of this method is that it finds the storm centre as well as the instantaneous forward speed of the storm, which is required later on in this study. Due to the nonlinearity of this method, it is more computationally expensive than the WC method.

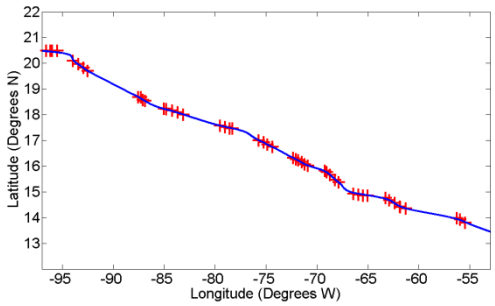

FIG. **2: Tropical cyclone centres (+) and track for Hurricane Dean (2007) using the TPF method.**

The TPF algorithm relies on the observation that pressure decreases as the radial distance from the centre of the storm is decreased. Many parametric models exist that can predict pressure profile of a tropical cyclone based upon certain characteristics. The TPF algorithm finds the parameters for the Holland pressure profile (1980, henceforth referred to as HPP) based upon the pressures obtained from the reconnaissance flight data. The HPP was chosen because it relies on only four parameters, has been widely validated and its limitations are well known (Kepert 2005). The four parameters used in the HPP are the shape parameter, b, the radius to maximum winds, r_m, the wind speed at RMW, v_m, and the pressure at the centre of the storm, p_c. The HPP also depends on the radial distance from the centre of the storm, r, which can be used to determine the location of the centre of the storm. The HPP is given below:

$$p_H(r) = p_c \left(1 + \frac{v_m^2 \exp\left(1 - \frac{r_m}{r}\right)^b}{b R_d T_v - v_m^2}\right) \quad (10)$$

where R_d is the gas constant for dry air and T_v is the virtual temperature, which is obtained from the reconnaissance flight data.

The TPF algorithm uses the HPP to minimize the cost function, which is given by:

$$J(\beta, a) = \sum_{i=1}^{\#\ of\ observations} \frac{\left(p_i - p_{H,i}(\beta, a)\right)}{\sigma_{p_i}^2} \quad (11)$$

where p_i is the observed pressure, $\beta = \{v_m, r_m, b, p_c\}$ and $a = \{x_C, y_C, u_C, v_C\}$, with (u_C, v_C) representing the velocity of the centre of the storm.

In order to minimize (11), it is differentiated with respect to β and a, and these differential equations are set to 0. This yields 8 non-linear equations which can be solved using numerical methods. The Levenberg-Marquadt (LM) algorithm for non-linear least squares has been used to solve for the unknown parameters. The LM method is used because all of

the unknown parameters are differentiable with respect to (11), which makes the LM method more efficient than Gauss Newton (Kepert 2005).

A comparison of the two methods showed that the TPF method was able to produce reasonable storm centres for a data acquisition frequency of up to 0.0167 Hz, whereas it was found that WC required a frequency of 1 Hz. The majority of the reconnaissance flight data available had a frequency of 0.1 Hz, so the TPF method was chosen.

The testing of the frequency stability was done by determining centres of data with a frequency of 1 Hz, which was the highest data frequency, and then finding the centres using the same data but resampled to 0.1 and 0.0167 Hz.

To ensure that the tracks were exhibiting realistic behaviour, they were compared with the National Hurricane Center's (NHC) Best Track Database (BTD), which compiles the centre fixes for tropical cyclones ever six hours with a tenth of a degree resolution. This level of resolution for time and for location does not provide enough accuracy to transform the reconnaissance data from earth relative to storm relative coordinates.

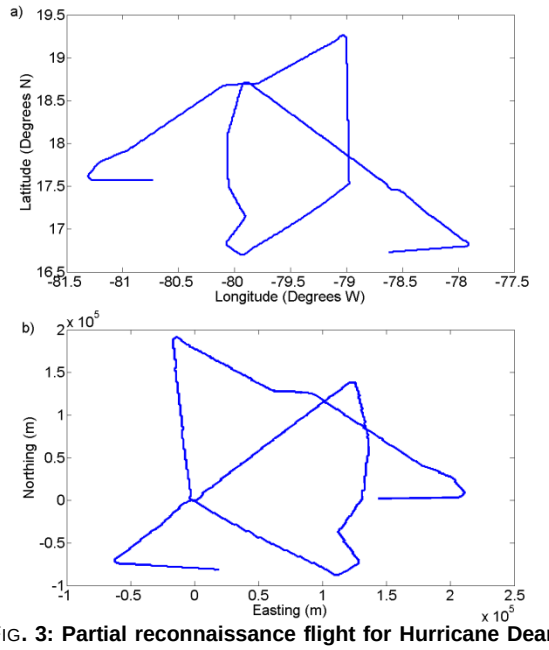

FIG. **3: Partial reconnaissance flight for Hurricane Dean, 20 August 2007 in a) earth relative, latitude/longitude coordinates and b) storm relative, easting/northing coordinates.**

Implementing the TPF method yields individual centre fixes with latitude, longitude, date and time associated to the fixes. In order to create a continuous track connecting the individual fixes together, a piecewise spline fit was used with a time step of 1 second. This meant that the location of the centre of the storm could be determined relative to the reconnaissance flight data. In order to transform the reconnaissance flight data from earth relative, latitude/longitude, coordinates to storm relative, easting/northing, coordinates, the Azimuthal Equidistant projection was utilized. This gave each data point a distance in meters how far north and east it was of the centre of the storm at that given time.

The wind speeds and directions obtained from the reconnaissance flights are also in terms of earth relative coordinates and need to be transformed into storm relative. To do this, it is required to subtract the storm speed and direction that were yielded from the TPF method from the raw velocity data. This yields wind speeds and directions relative to the storm centre, not to the earth.

3. OBJECTIVE ANALYSIS

The primary direction of the flow is in the tangential direction and as such it was beneficial to convert the coordinate system a final time from Cartesian to Cylindrical. In this cylindrical coordinate system, the data has been rotated so that it is orientated with the direction that the centre of the storm is traveling. This means that 0° is the direction that the storm is traveling in, and angles increase positively in the clockwise direction.

Two methods were used to create a two dimensional field. The first was outlined by Mueller et al. (2005) and is based upon an objective analysis method described by Thacker (1988). In the Mueller/Thacker (MT) method, the error between the raw data and the analyzed field is minimized while the smoothness of the analyzed field is maximized, concurrently. The amount of smoothness is controlled by parameters set in the algorithm. The combination of smoothness and minimization of error was unique to this method and had been used by Mueller et al. for a very similar purpose as of this study.

The MT method minimizes the following cost function:

$$C = \frac{1}{2}\sum_{k=1}^{K}(u_k - U_k)^2 + \sum_{i=1}^{I}\sum_{j=1}^{j}\left[\alpha\left(\delta_{rr}U_{ij}\right)^2 + \beta\left(\delta_{\theta\theta}U_{ij}\right)^2\right] \quad (12)$$

where u_k is the raw data, U_K is the interpolated value from the grid at the location of u_k, K is the number of reconnaissance flight data points, U_{ij} is the grid data at point (i,j), α and β are smoothing parameters, I is the number of grid data points in the radial direction and J is the number of grid data points in the tangential direction. δ_{rr} and $\delta_{\theta\theta}$ are the discretized second derivative operators in the radial and tangential directions, respectively. When δ_{rr} and $\delta_{\theta\theta}$ are applied to U_{ij}, they yield:

$$\delta_{rr}U_{ij} = (U_{i+1,j} + U_{i-1,j} - U_{i,j})/\Delta r^2 \quad (13)$$

$$\delta_{\theta\theta}U_{ij} = r^2(U_{i,j+1} + U_{i,j-1} - U_{i,j})/\Delta\theta^2 \quad (14)$$

In the MT method, the k terms control the error between the raw data and the grid data and the (i,j) terms control the smoothness of the gridded data.

The Barnes algorithm was the second objective analysis method investigated. Parameters outlined by Benjamin and Seaman (1985) were used in the implementation as they had been optimized for curved flow. The advantage of the Barnes algorithm is that it

is computationally inexpensive as compared to the MT method. Error minimization is achieved by enforcing a radius of influence on a grid point where raw data close to a grid point have greater influence on it than the raw data far away from the grid point. Smoothness is achieved in Benjamin and Seaman's implementation by having an elliptical rather than circular radius of influence, with the semi-major axis in the azimuthal direction and the semi-minor axis in the radial direction. The ellipse is also curved, resembling the shape of a banana. This increases smoothing in the azimuthal direction by increasing the influence of the raw data in this direction and decreases the smoothing in the radial direction by decreasing the influence of the raw data in the radial direction.

The weighting function, w_{ij}, is given by:

$$w_{ij} = \begin{cases} \frac{R^2 - d_m^2}{R^2 + d_m^2} & for\ d_m^2 < R^2 \\ 0\ for\ d_m^2 \geq R^2 \end{cases} \quad (15)$$

$$d_m = \left[\frac{r_k^2 (\theta_k - \theta_{ij})^2}{E_k^2(|U_{ij}|)} + \left(|r_k| - r_{ij}\right)^2 \right]^{\frac{1}{2}} \quad (16)$$

where d_m is the distance from point m to the grid point at (i,j), r_k is the radius of curvature at data point k, r_{ij} is the distance from U_{ij} the centre of curvature, C_k, E_k is Cressman's isotropic function, U_{ij} is as in (12), the , θ_k is the azimuthal angle of curvature to point k, θ_{ij} is the azimuthal angle of curvature to point (i,j) and R is an arbitrary radius of influence, set to 20 km for this application. The weighting function is used in the Barnes algorithm to find U_{ij}, given as:

$$U_{ij} = \frac{\sum_{k=1}^{K} w_{ij}\, u_k}{\sum_{k=1}^{K} w_{ij}} + \frac{\sum_{k=1}^{K} w_{ij}\, (u_k - U_{k,0})}{\sum_{k=1}^{K} w_{ij}} \quad (17)$$

where $U_{k,0}$ is the initial guess for the field, which was taken to be the azimuthal average of the quantity being objectively analyzed.

A qualitative comparison showed little difference in error between the gridded and raw data for both methods. In the areas that data was present, the gridded data matched the raw data quite well. The differences came in the smoothness and curved nature of the data. The Thacker method was able to produce fields that were sufficiently and realistically curved, whereas the Barnes algorithm produced fields that resembled squares with rounded edges. Although the Benjamin and Seaman implementation of the Barnes method was specifically for curved systems, it did not fully capture the curved nature of the geopotential field.

The MT method was utilized as it provided a more realistic representation of the geopotential field.

The velocity and geopotential fields were both objectively analyzed. The error between the raw geopotential data and the objectively analyzed field was minimal, with a mean average of about 0% and a standard deviation of about 2% for radii from 0 to 200 km. The grid was split into 16 sections in the azimuthal direction and 40 sections in the radial direction.

A direct comparison of the error of the geopotential and velocity fields is not possible because of the differences in magnitudes for geopotential and velocity values. Typical velocities are on the order of 30 m/s where as typical geopotential values are on the order of 3000 m. Velocities at the centre of a storm approach 0, increasing the percentage error dramatically, with some individual error points reaching higher than 1000%.

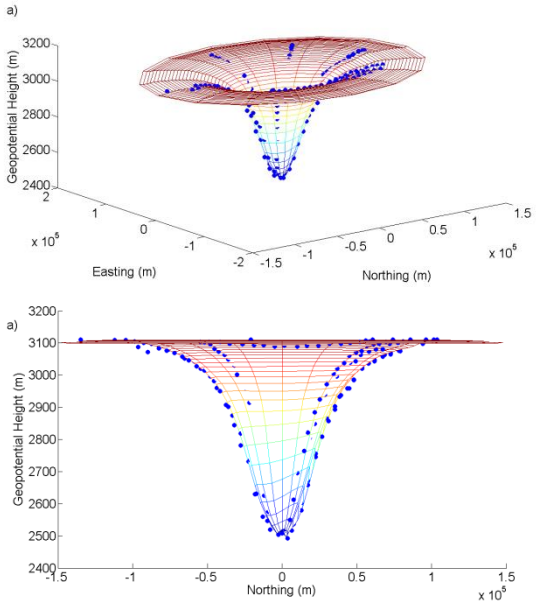

FIG. **4: Objectively analyzed geopotential field plotted with raw data (•) used to create the field. Hurricane Dean, 20 August 2007.**

The result of this error level issue was that the velocity fields were visually inspected so that poor fits were removed from the data set.

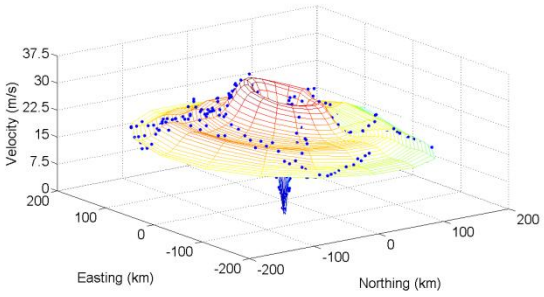

FIG. **5: Objectively analysed tangential velocity field with raw data (•) plotted. Hurricane Dean, 20 August 2007.**

4. GRADIENT BALANCE CALCULATIONS

Using (1) and (2), the gradient balance velocities could be calculated based upon the objectively analyzed geopotential field. These gradient balance velocities were then compared to the objectively

analyzed velocity fields and gradient balance was quantified.

The presence or lack of gradient balance has been noted according to the following characteristics: the quadrant of the storm, the strength of the storm and the change in strength of the storm. The error was plotted with respect to radius as well as the ratio between radius and RMW. This was in order to test one of Gray's arguments that RMW should be incorporated into the analysis.

Willoughby (1990, 1991) plotted error with respect to radius and found that when the geopotential field has been averaged azimuthally, storms were in gradient balance. Gray's (1991) counter argument to this was that the geopotential field should not be averaged azimuthally and that the error should be plotted with respect to the RMW.

The error threshold for gradient balance in this study has been set to ±5%. When a percentage difference between the objectively analyzed tangential velocity field and the gradient velocity based upon the objectively analyzed geopotential field is less than ±5%, a storm is said to be in gradient balance. A value of ±5% was chosen due to the error introduced through objective analysis as well as data collection.

The current study has found that gradient balance is a common characteristic among most storms. Of the 44 objectively analyzed fields that were investigated, it was found that 30 exhibited gradient balance in at least one quadrant.

When gradient balance is characterized by quadrant, 63% of the quadrants investigated exhibited gradient balance, with 64% in the front right quadrant, 71% in the rear right quadrant, 57% in the rear left quadrant and 57% in the front left quadrant. Considering the sample size, it is safe to conclude that the quadrant has little to no effect on the presence of gradient balance. Statistically, the likelihood of observing gradient balance is equal for all of the quadrants.

When gradient balance is characterized according to radius, a well defined region where gradient balance is likely to occur emerges. Whenever gradient balance was encountered, a range was recorded, the radius at which gradient balance appears and the radius at which gradient balance disappears. In order to be considered gradient balance, this range was required to be a minimum of 25 km or 2 RMWs. On average, this range is from 8 km from the centre of the storm to 88 km. Likewise, for the ratio between radius and radius to maximum wind the range is 0.4 to 6.8 RMWs. Figure 6a shows error plotted against radius and Fig. 6b shows error plotted against RMW. There is no discernable difference between these plotting methods so it can be concluded that analysis completed using either method is valid.

For both cases, the reasons why gradient balance is not present beyond the ranges is known. For the values less than 8 km and 0.4 RMW, tangential velocities are low. This means that a small difference (on the order of 1 m/s) between the calculated gradient balance velocity and the actual velocity will lead to a large percentage difference. For values greater than 88 km and 6.8 RMW the reason is because the calculation of the gradient balance velocity begins to breakdown as the radius increases. When (1) and (2) are solved for v, the r term becomes dominant for large values of r. Any small inaccuracies in the geopotential gradient become amplified.

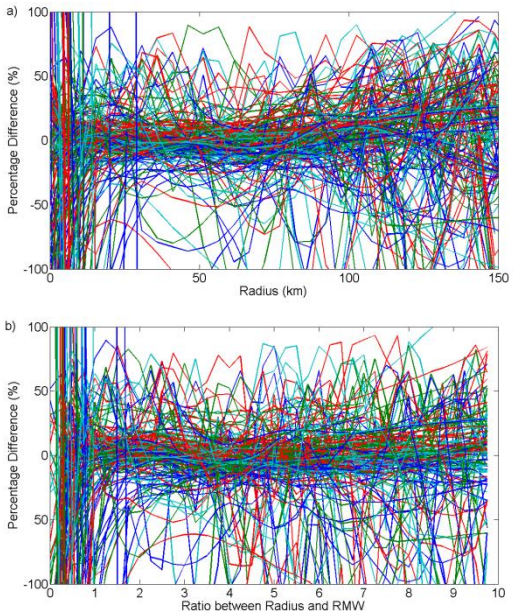

FIG. **6: Percentage error between tangential velocity and gradient velocity. Error has been plotted by a) radius and b) RMW. The front right quadrant has been plotted in blue, the rear right quadrant has been plotted in green, the rear left quadrant has been plotted in red and the front left quadrant has been plotted in cyan.**

Figures 7 a) to d) show the percentage error classified by quadrant. Fields that are in gradient balance for a radial distance greater than 25 km have been indicated in blue. The error characteristics are similar across the four quadrants. Error was plotted versus radius in the region where gradient balance was most likely to occur: 8 to 88 km.

The strength of the storm has been classified using the central pressure of the storm. The average central pressure of storms in gradient balance is 960 hPa and the average central pressure of storms not in gradient balance is 970 hPa. Due to the relatively small sample size used in this study, this difference of 10 hPa cannot be concluded as statistically relevant. Thus, based on this small difference in pressure, it is not possible to determine the effect of storm strength on gradient balance within the storm.

The final storm characteristic that has been investigated is the change in the strength of the storm. This has been measured by looking at the change in the central pressure of the storm. If the central pressure is decreasing by a rate greater than 4 hPa over 6 hours, the storm is said to be strengthening and if the central pressure is increasing by a rate greater than 4 hPa the storm is said to be weakening. If the central pressure is changing by less than 4 hPa, the storm is said to be steady.

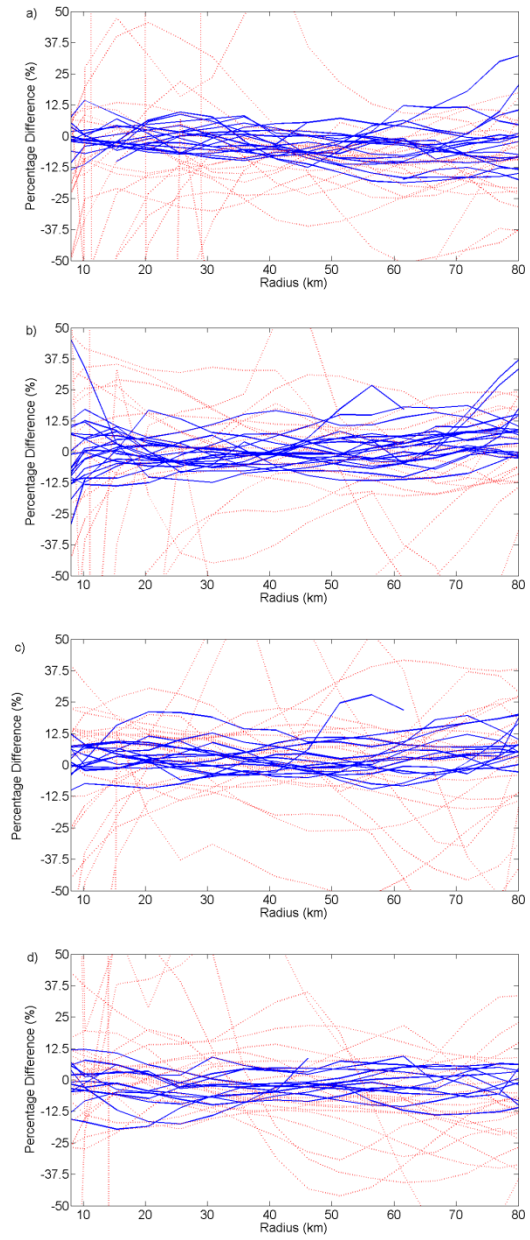

FIG. **7: Percentage error plotted against radius for the a) front right, b) rear right, c) rear left and d) front left quadrants. Fields in gradient balance for a minimum of 25 km are plotted with a solid blue line and fields not in gradient balance are plotted with a dashed red line.**

TABLE **1: The impact of the change in the strength of a storm on gradient balance.**

	Strengthening	Steady	Weakening
Entire Set	20	12	12
In Gradient Balance	13	8	9
Out of Balance	7	4	3

There does not seem to be any increase in gradient balance for strengthening, weakening or steady storms. All three characteristics result in gradient balance 65 to 75% of the time.

5. FUTURE WORK

In order to gain more confidence in the work up to this point and to gain more insight into gradient balance characteristics, the number of storms being investigated will be expanded to 30 within the same 2002-2008 time period. The inclusion of more data will allow different categories to be combined in the analysis, such as looking at strong storms that are weakening.

6. AKNOWLEDGEMENTS

The authors would like to acknowledge the computing resources graciously provided by SHARCNET. SHARCNET (www.sharcnet.ca) is a consortium of colleges, universities and research institutes operating a network of high-performance computer clusters across Ontario.

7. REFERENCES

Benjamin, S. G. and N. L. Seaman, 1985: A simple scheme for objective analysis in curved flow. *Mon. Wea. Rev*., 113, 1184-1198

Gray, W. M., 1991: Comments on "Gradient balance in tropical cyclones." *J. Atmos. Sci.*, 48, 1201–1208.

Kepert, J. D., 2005: Objective analysis of tropical cyclone location and motion from high-density observations. *Mon. Wea. Rev.*, 133, 2406–2421.

———, 2006a: Observed boundary layer wind structure and balance in the hurricane core. Part I: Hurricane Georges. *J. Atmos. Sci.*, 63, 2169–2193.

———, 2006b: Observed boundary layer wind structure and balance in the hurricane core. Part II: Hurricane Mitch. *J. Atmos. Sci.*, 63, 2194–2211.

Mueller, K. J., M. DeMaria, J. Knaff, J. Kossin, and T. H. Vonder Haar, 2006: Objective estimation of tropical cyclone wind structure from infrared satellite data. *Wea. Forecasting*, 21, 990–1005.

Thacker, W. C., 1988: Fitting models to inadequate data by enforcing spatial and temporal smoothness. *J. Geophys. Res.*, 93, 10655–10665.

Willoughby, H. E., 1990: Gradient balance in tropical cyclones. *J. Atmos. Sci.*, 42, 265–274.

———, 1991: Reply. *J. Atmos. Sci*., 48, 1209–1212.

———, and M. B. Chelmow, 1982. Objective determination of hurricane tracks from aircraft observations. *Mon. Wea. Rev.*, 110, 1298–1305.